J Adv Ceram

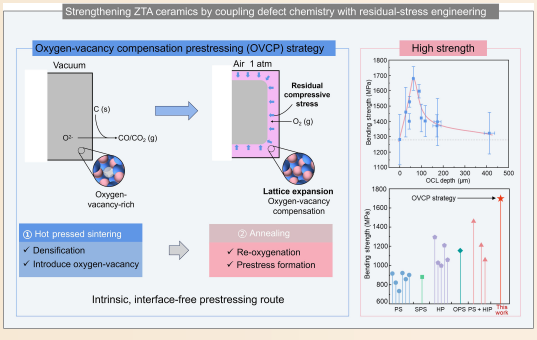
Research Article

# Intrinsic surface prestressing via oxygen-vacancy regulation enables high-strength ZTA ceramics

Shile Chen[1,†], Wenkai Fan[1,2,†], Liping Chai[3], Jing Xia[1], Honghua Li[1,✉], Jiangtao Li[1,2,✉]

Cite this article: Chen S, Fan W, Chai L, et al. *J Adv Ceram* 2026, **15**(8): 9221346. https://doi.org/10.26599/JAC.2026.9221346

**ABSTRACT:** Introducing a surface compressive stress layer is an effective way to enhance the strength of brittle ceramics, yet achieving such prestressing intrinsically in monolithic oxide ceramics remains challenging. Here, we report a novel method called oxygen-vacancy compensation prestressing (OVCP) to generate *in situ* surface prestressing in zirconia-toughened alumina (ZTA) ceramics. Oxygen vacancy-rich ZTA was first produced by vacuum hot pressing, followed by air annealing to induce surface reoxygenation and form an oxygen-charged layer (OCL). The optimized treatment increased the flexural strength to (1679±78) MPa, representing a 31% improvement over the unannealed state. Oxygen-vacancy compensation during annealing induces lattice expansion in the near-surface region. Constrained by the less-oxidized interior, this lattice expansion is converted into a residual compressive stress field that suppresses bending-induced failure. A simplified bilayer model quantitatively supports the experimentally observed strengthening behavior. These findings establish oxygen vacancy-regulated lattice expansion as an effective mechanism for intrinsic surface prestressing and provide a simple, interface-free route for strengthening oxide ceramics.




**KEYWORDS:** zirconia-toughened alumina (ZTA); flexural strength; heat treatment; prestressed ceramics

## 1 Introduction

Zirconia-toughened alumina (ZTA) ceramics are among the most important structural oxide ceramics because they combine high hardness, chemical inertness, and outstanding fracture resistance. These attributes have enabled their widespread use in demanding applications, ranging from high-precision cutting tools and wear-resistant industrial components to load-bearing biomedical implants such as femoral heads for total hip arthroplasty [1,2]. As performance requirements continue to increase in both engineering and clinical settings, further improvement in the strength of ZTA, particularly its flexural strength, remains a longstanding objective. To date, strengthening of ZTA has been pursued primarily through bulk microstructural design, including transformation toughening, grain-boundary engineering, and second-phase reinforcement. Although these approaches have led to state-of-the-art flexural strengths exceeding 1 GPa, further gains are becoming increasingly difficult to realize [3–5]. However, these bulk-dominated strategies are approaching a regime of diminishing returns: additional strength gains increasingly rely on highly complex processing or finely tuned dopant design, often at the expense of economic feasibility and long-term reliability [6–8].

Surface prestressing offers a fundamentally different route to strength enhancement by introducing a residual compressive layer that offsets externally applied tensile stress [9,10]. In principle, such a stress field can markedly increase the apparent flexural strength of brittle ceramics by suppressing surface crack initiation. Existing approaches mainly rely on external coatings or laminated architectures with tailored thermal-expansion mismatch. While effective, these methods inherently involve heterogeneous interfaces and therefore suffer from reliability concerns such as delamination, interfacial debonding, and thermally induced stress concentration [11–13]. Classical studies on brittle coating systems have shown that thermal and elastic mismatch can promote interfacial crack initiation, delamination, and even spallation, thereby degrading the retained prestress and structural reliability [14]. Likewise, in layered/bilayer ceramic architectures, residual-stress-induced debonding of the surface layer has been identified as a major failure mode [15].

Developing an intrinsic, interface-free mechanism to generate surface compression directly within monolithic ZTA is therefore both scientifically compelling and technologically important.

A promising route is to exploit the intrinsic coupling between point defects and the lattice state in oxide ceramics. In ZTA-

† Shile Chen and Wenkai Fan contributed equally to this work.

[1] Key Laboratory of Cryogenic Science and Technology, Technical Institute of Physics and Chemistry, Chinese Academy of Sciences, Beijing 100090, China. [2] University of Chinese Academy of Sciences, Beijing 100049, China. [3] Hebei Ruihe Medical Devices Co., Ltd., Shijiazhuang 050035, China.

✉ Corresponding authors. E-mail: H. Li, lihonghua@mail.ipc.ac.cn; J. Li, lijiangtao@mail.ipc.ac.cn

Received: April 30, 2026; Revised: July 3, 2026; Accepted: July 5, 2026

© The Author(s) 2026. This is an open access article under the terms of the Creative Commons Attribution 4.0 International License (CC BY 4.0, http://creativecommons.org/licenses/by/4.0/).

related phases, oxygen nonstoichiometry is closely linked to lattice strain; therefore, regulating oxygen vacancies offers a pathway to internal stress engineering [16–18]. We hypothesize that if an oxygen-vacancy gradient is first created and then selectively compensated near the surface through oxygen diffusion, the associated constrained lattice expansion can produce robust *in situ* surface compressive stress. This oxygen-charged layer (OCL) is expected to avoid the interface liabilities of conventional coatings while providing effective strengthening.

Here, a novel strengthening technique, designated oxygen-vacancy compensation prestressing (OVCP), is introduced. A high concentration of oxygen vacancies was first introduced by vacuum hot-press sintering, followed by air annealing to drive surface reoxygenation and form an oxidized compressive layer. By systematically varying the annealing temperature and time, we clarify the time–temperature equivalence governing OCL development and reveal the underlying strengthening mechanism. The optimized ZTA exhibits a flexural strength of approximately 1679 MPa, substantially exceeding that of the unannealed state. Moreover, a quantitative bilayer model is developed to correlate OCL thickness and chemical expansion with the magnitude of the surface compressive stress and the observed strength evolution. This work establishes a defect engineering paradigm for achieving ultrahigh-strength oxide ceramics through intrinsic, *in situ* surface prestressing.

## 2 Experimental

### 2.1 Preparation of surface prestressing ZTA samples

Commercial granulated ZTA powder (median particle size $D_{50}$ = 120 nm; ZTA80D1-WL, Baikowski, France) was used as the starting material. The chemical composition (mass fraction) was: $Al_2O_3$ 71.4%, $ZrO_2$ 25.5%, $Y_2O_3$ 1.41%, $HfO_2$ 0.55%, SrO 0.75%, and $Cr_2O_3$ 0.28%. Bulk ZTA ceramics were fabricated by vacuum hot pressing (ZT-40-20Y, Shanghai Chenhua Science Technology Co., China) in a graphite die at 1550 °C under 30 MPa for 2 h. The sintered bodies were machined into bar specimens with dimensions of 3 mm × 4 mm × 36 mm and subsequently polished according to ISO 14704:2000.

The machined specimens were then annealed in air in a muffle furnace (SSJ-17, Luoyang Shenjia Kiln Industry Co., China) at 900–1300 °C for 0.5–8 h. As control groups, samples without annealing (NA) and fully annealed (FA) were prepared simultaneously. The FA sample was obtained by heat treatment at 1400 °C for 8 h.

### 2.2 Characterization

The relative density of the ZTA ceramics was measured with Archimedes' method. The three-point flexural strength of the samples was measured on a universal testing machine (DZS-III, CTC, China) at a crosshead speed of 0.5 mm/min with a support span of 30 mm. At least five samples were tested for each group. During three-point bending, the polished surface containing the OCL was placed on the tensile side. Since the specimens were annealed after machining and polishing, OCL was formed on all external surfaces. The tensile surface during bending therefore contained the OCL, allowing the residual compressive stress to counteract the externally applied tensile stress. The Vickers hardness of the samples was measured by the indentation method (HVS-1000, Shanghai Zhongyan Instrument Co., Ltd., China) with an applied load of 1 kgf for 15 s. Cross-sectional optical images were obtained using an optical microscope (RY-605, Shanghai Renyue, China). Microstructural observations were conducted using a scanning electron microscope (SEM; QUANTA FEG-250, Thermo Fisher Scientific, USA). The coefficient of thermal expansion (CTE) was measured using a dilatometer (DIL 402C, NETZSCH, Germany).

Phase assemblage was analyzed by an X-ray diffractometer (XRD; D8 ADVANCE, Bruker, Germany) with Cu Kα radiation, and the diffraction data were refined using Profex 5.7. Oxygen vacancy-related defects were probed by an electron paramagnetic resonance spectrometer (EPR; E 500, Bruker, Germany). Surface chemical states were characterized by an X-ray photoelectron spectrometer (XPS; ESCALAB 250Xi, Thermo Fisher Scientific, USA).

## 3 Results and discussion

### 3.1 Formation of OCL under post-annealing

The OVCP strategy is illustrated in Fig. 1(a). Vacuum hot-press sintering simultaneously achieves densification (the relative density of the as-sintered ZTA reached 99.7%, indicating nearly full densification) and introduces a high concentration of oxygen vacancies under reducing conditions imposed by the vacuum/graphite environment, yielding a gray-black as-sintered ZTA. Subsequent annealing in air drives surface reoxygenation and forms an OCL, accompanied by surface prestressing.

In the cross-sectional images (Fig. 1(b)), a pink outer region is clearly observed after annealing and progressively advances inward, forming a distinct core–shell structure. This color evolution is consistent with progressive surface reoxidation: the as-sintered material, produced in a low-oxygen-potential vacuum/graphite environment, contains a high concentration of oxygen vacancy-related defects, whereas annealing in air compensates for these defects near the surface. The final pink coloration is also influenced by the presence of $Cr^{3+}$ dissolved in the $Al_2O_3$ matrix. Quantitatively, the OCL depth $d$ increases with both temperature and time. At fixed annealing time $t = 1$ h, $d$ follows an exponential (Arrhenius-like) dependence on temperature (Fig. 1(c)). At a fixed temperature of 1273 K, $d$ follows a sublinear power law with time (Fig. 1(d)), indicating diffusion-controlled oxygen ingress. These relationships are consistent with a thermally activated one-dimensional Fick-type process. The apparent oxygen-diffusion activation barrier in ZTA is estimated to be 2.0 eV (Fig. S1 in the Electronic Supplementary Material (ESM)). This value is much lower than that reported for polycrystalline $Al_2O_3$ (6–7 eV) and closer to that of polycrystalline yttria-stabilized zirconia (YSZ; 0.8–1.5 eV), despite $Al_2O_3$ being the major phase, but it is governed faster along $ZrO_2$ regions and $Al_2O_3$–$ZrO_2$ heterointerfaces (short-circuit diffusion). Practically, this diffusion-controlled growth provides a direct time–temperature-processing map for tailoring the OCL thickness and, consequently, the prestressing state.

### 3.2 Enhanced flexural strength via stress generation in the shell layer

Figure 2 examines the local mechanical response across the cross-section of the sample (annealed at 1100 °C for 1 h) by Vickers indentation in the OCL and the core. As shown in Fig. 2(a), the measured hardness values are (19.81±0.15) GPa (OCL) and (19.96±0.42) GPa (core), indicating no statistically meaningful hardness change after annealing within the experimental scatter. Thus, the heat treatment primarily modifies the stress state rather than intrinsic local hardness.

In contrast, the crack morphology around the indents differs

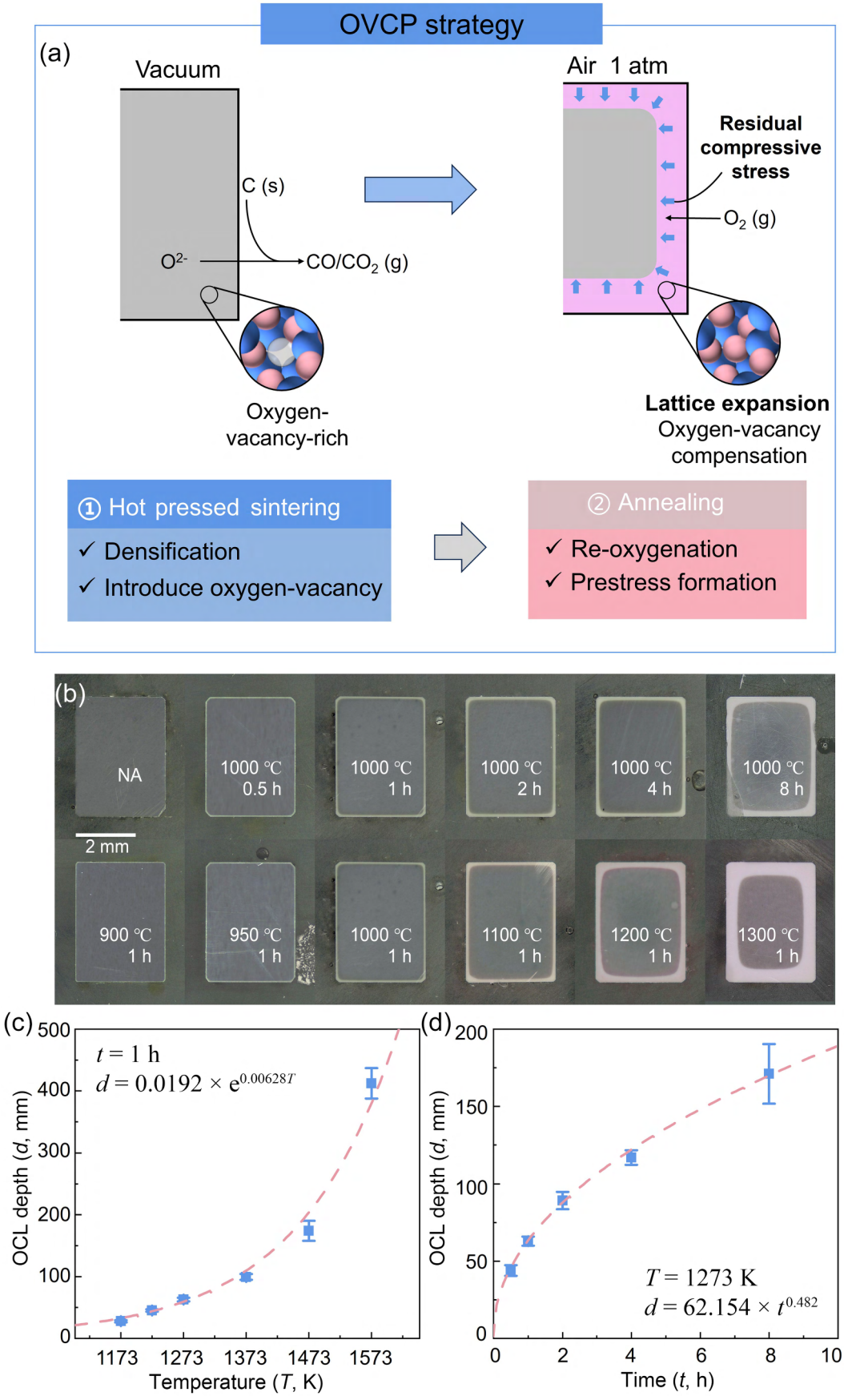



**Fig. 1** (a) Schematic diagrams of OVCP strategy. (b) Cross-sections of samples heat-treated under different conditions. (c) Relationship between OCL depth (*d*) and temperature (*T*). (d) Relationship between OCL depth (*d*) and time (*t*).


清華大学出版社 Tsinghua University Press | SciOpen

markedly between the two regions (Figs. 2(b) and 2(c)). The core exhibits a nearly symmetric crack pattern, with comparable crack extension along different directions. The OCL shows clear directional anisotropy (crack lengths as shown in Table S1 in the ESM): crack growth is promoted along one principal direction and suppressed along the orthogonal direction (defined as radial/axial in Fig. 2(a)), evidencing a residual-stress field. Following the coordinate definition in Fig. 2(a) and the schematic in Fig. 2(d), this behavior is consistent with radial tensile stress and axial compressive stress in the OCL. Mechanistically, such a biaxial stress state is expected from constrained lattice/volume changes during surface reoxygenation: In-plane compression in the surface layer is balanced by tensile stress along the normal direction. These indentation-crack signatures therefore provide direct mechanical evidence for the formation of a designed prestressed surface layer in ZTA.

The macroscopic consequence of this surface stress field is reflected in the three-point flexural strength. Figure 3(a) summarizes the dependence of the three-point flexural strength on the thickness of the prestressed layer. As the prestressed layer depth ($d$) increases, the flexural strength exhibits a nonmonotonic evolution, characterized by an initial rapid increase followed by a gradual decrease. The maximum flexural strength, (1679.4±77.6) MPa, is obtained at $d \approx 62.9$ μm, which represents an improvement of approximately 31% over the unannealed sample. Beyond this critical depth, the strength decreases progressively and ultimately converges toward the level of the unannealed group. Notably, although the annealing

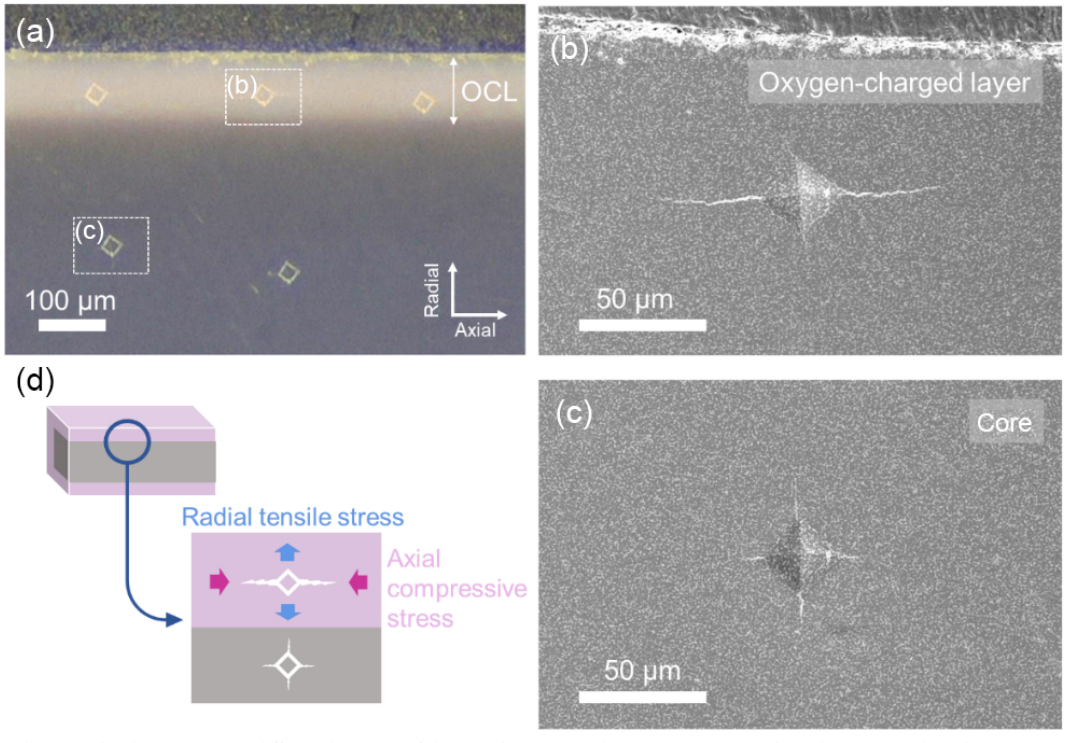



**Fig. 2** Vickers indentation hardness testing at different locations of the sample: (a) optical microscopy image, (b) indentation and cracks in oxygen diffusion layer, (c) indentation and cracks in core region, and (d) schematic illustration of stress distribution within oxygen diffusion layer.

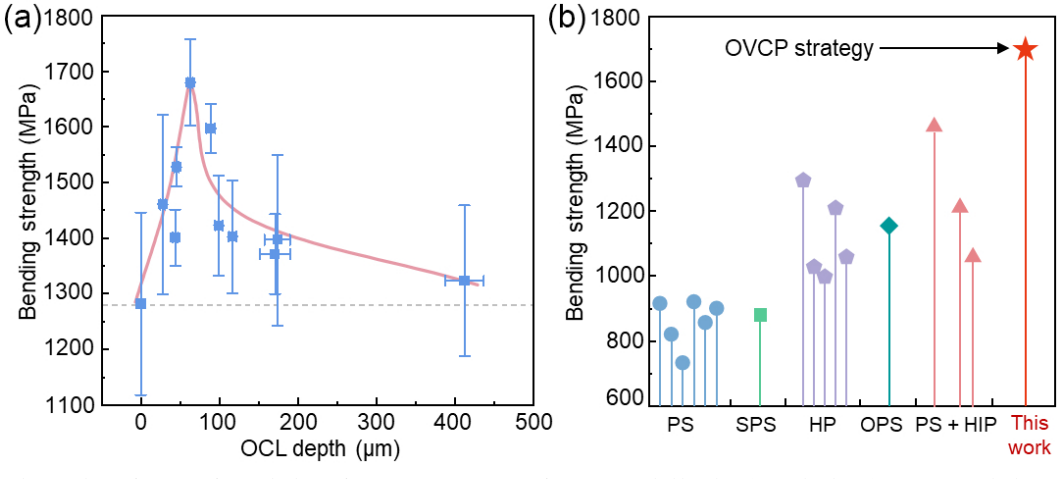



**Fig. 3** (a) Flexural strength as a function of OCL thickness for 11 specimens ranging from unannealed baseline (OCL depth = 0) to progressively deeper OCLs produced under different annealing conditions (temperature: 900–1300 °C; holding time: 0.5–8 h). (b) Comparison of flexural strength of ZTA material obtained in this study with previously reported data for ZTA ceramics fabricated by different sintering methods (PS: pressureless sintering; SPS: spark plasma sintering; HP: hot pressing; OPS: oscillatory pressure sintering; PS + HIP: pressureless sintering + hot isostatic pressing) [3–6,19–29].

treatments were conducted under different temperature and time conditions, all data points approximately fall on the same trend curve. This suggests that the flexural strength is governed primarily by the OCL depth rather than by the specific annealing temperature or time alone. In other words, similar strengthening effects can be achieved when comparable OCL depths are produced through different combinations of temperature and holding time, revealing an apparent time–temperature equivalence in the evolution of flexural strength.

As shown in Fig. 3(b), the mechanical properties of ZTA ceramics produced by different sintering strategies were further compared [3–6,19–29]. The optimized OVCP-ZTA reaches a flexural strength comparable to the highest values reported for hot isostatic pressing (HIP)-treated ZTA ceramics, but it achieves this enhancement through intrinsic surface prestressing rather than relying solely on bulk densification or microstructural refinement. A simple two-step heat-treatment process was sufficient to generate *in situ* surface prestress, resulting in a substantial increase in flexural strength. In contrast to conventional strengthening strategies, the present approach introduces a fundamentally different paradigm by exploiting intrinsic residual stress at the surface. From this perspective, the proposed method highlights the potential of defect engineering-assisted prestress modulation as an effective route toward high-strength ZTA ceramics.

### 3.3 Mechanism of strain layer formation and surface stress induction

To clarify the intrinsic mechanism responsible for the strength enhancement, the oxygen vacancies were first examined. As shown in Fig. 4, the unannealed sample displays a strong EPR response characteristic of oxygen vacancy-related defects, evidencing the existence of a high concentration of oxygen vacancies in the as-sintered ZTA ceramic. After annealing, the signal intensity decreases substantially, demonstrating effective defect compensation during oxidation in air.

Consistent with the EPR results, XPS characterization further reveals distinct differences in the surface chemical states of the NA and FA samples (Fig. 5). The O 1s spectra (Fig. 5(a)) can be fitted with two components located at 530.9 and 532.2 eV, corresponding to lattice oxygen and surface active oxygen, respectively [30]. The NA sample contains a markedly higher fraction of the nonlattice oxygen component than the FA sample, suggesting a higher density of oxygen vacancy-associated surface defects prior to annealing. In the Zr 3d spectra (Fig. 5(b)), the NA sample exhibits both peak broadening and a slight shift toward lower binding energy, implying partial reduction of $Zr^{4+}$ to $Zr^{(4-x)+}$ under the reducing conditions imposed by the graphite environment during hot pressing. This strongly supports the generation of oxygen vacancies in the zirconia phase. In contrast, the Al 2p spectra remain essentially unchanged after annealing, implying that the dominant redox-active defect response occurs in the zirconia phase, whereas alumina remains comparatively stable (Fig. S2 in the ESM). For samples annealed under intermediate conditions, the oxygen vacancy-related XPS signals decrease progressively with increasing annealing severity, indicating gradual defect compensation during reoxidation (Fig. S3 in the ESM). This trend is consistent with the measured increase in OCL thickness, further supporting that the compressive layer develops as oxygen vacancies are progressively compensated. Then, possible microstructural contributions were also examined. Cross-sectional SEM observations of polished, unetched specimens before and after annealing at 1300 °C reveal no discernible grain coarsening in the OCL region (Fig. S4 in the ESM).

Taken together, these results show that hot pressing under low oxygen potential introduces oxygen vacancy-rich reduced states, particularly in the zirconia-containing regions, while subsequent air annealing compensates for those vacancies in the near-surface region. The OCL is thus fundamentally a reoxidized defect-gradient layer, and its formation is governed primarily by oxygen-vacancy compensation.

Upon annealing in air, oxygen penetrates into the surface region and fills the oxygen vacancies, thereby reversing the reduction-induced nonstoichiometry and restoring the surface toward an oxidized, near-equilibrium state. This reduced-to-

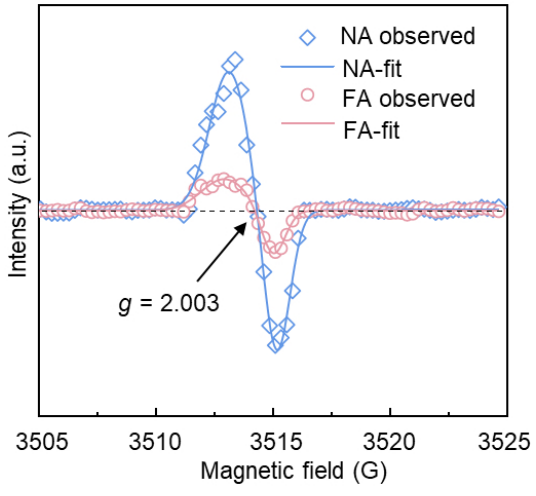



**Fig. 4** EPR spectra of NA and FA samples.

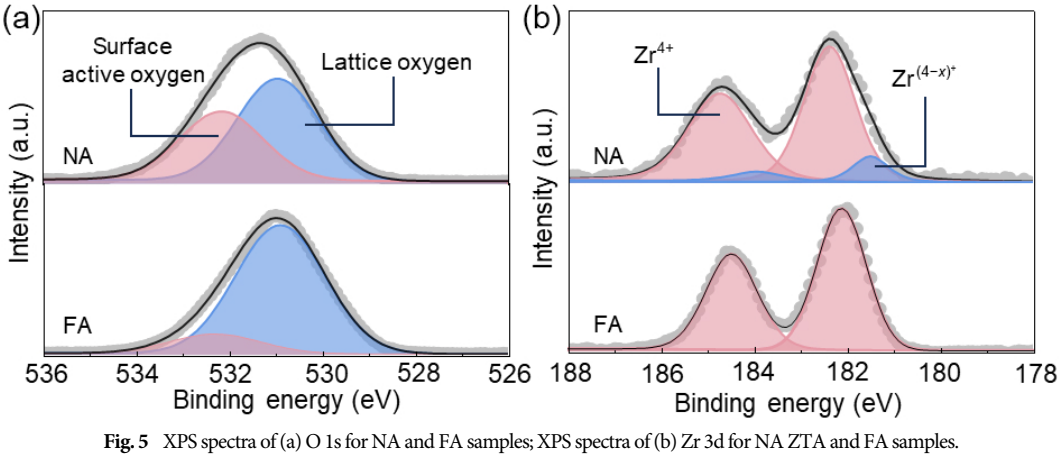



**Fig. 5** XPS spectra of (a) O 1s for NA and FA samples; XPS spectra of (b) Zr 3d for NA ZTA and FA samples.


清華大学出版社 Tsinghua University Press | SciOpen

oxidized transition is not only reflected in the observed color change but also plays a crucial role in the evolution of the surface stress state, thereby laying the foundation for the formation of the compressive prestressed layer.

Figure 6 presents the XRD patterns of the NA and FA samples. Both states are dominated by tetragonal zirconia (t-$ZrO_2$) and α-alumina (α-$Al_2O_3$), with only a minor fraction of monoclinic zirconia (m-$ZrO_2$). Compared with the NA sample, the FA sample exhibits discernible peak shifts (Fig. S5 in the ESM), suggesting that annealing induces changes in crystal lattice dimensions.

To further evaluate this effect, lattice parameters and unit-cell volumes were refined from the 2$\theta$ values of several high-angle reflections, as listed in Table 1. The results show that oxygen incorporation during annealing leads to an obvious expansion of the t-$ZrO_2$ lattice, corresponding to a unit-cell volume increase of approximately 0.364%. Meanwhile, the α-$Al_2O_3$ phase also undergoes lattice expansion, with a volume increase of approximately 0.319%. Although the constituent phases are crystallographically anisotropic, the hot-pressed ZTA is treated as a macroscopically quasi-isotropic polycrystalline composite for a first-order estimation because the grains are randomly oriented and no strong crystallographic texture is detected. The calculated expansion therefore represents an orientation-averaged effective chemical strain rather than the anisotropic lattice strain of individual grains. The average macroscopic volume expansion associated with this oxidation process is estimated to be approximately 0.340% based on the phase-volume-weighted contribution of the two major constituents.

The formation of the surface compressive layer originates from oxygen-vacancy compensation under mechanical constraints. During vacuum hot pressing, the low oxygen partial pressure drives oxygen loss from the lattice according to the defect equilibrium $O_O^{\times} \leftrightarrow V_O^{\cdot\cdot} + 2e' + \frac{1}{2}O_2$, producing a uniform distribution of oxygen vacancies throughout the specimen. Upon air annealing, the oxygen chemical potential gradient between the atmosphere and the interior drives inward diffusion. Since oxygen transport is kinetically limited, vacancy compensation proceeds preferentially near the surface, creating a compositional gradient. Filling oxygen vacancies causes lattice expansion (~0.11% linear strain).

The above structural evolution provides direct evidence that oxygen vacancy compensation is accompanied by measurable lattice dilation. In other words, the transition from the reduced state to the oxidized state generates an intrinsic expansion strain in the oxygen-penetrated region. Since this oxidized surface layer is constrained by the relatively unoxidized interior, the oxidation-induced expansion is mechanically restricted, leading to the development of a compressive residual stress field near the surface. Therefore, the residual compressive layer is essentially a consequence of constrained lattice expansion triggered by oxygen vacancy compensation. This constraint-generated expansion provides the physical origin of the prestressed surface layer.

To quantitatively describe the dependence of the residual surface stress on the OCL thickness, a simplified bilayer constraint model was developed (Fig. 7(a); the full derivation is provided in the ESM). The oxidized surface layer was assumed to undergo lattice expansion induced by oxygen-vacancy compensation, while the less-oxidized interior acted as a mechanical constraint. XRD patterns before and after annealing show no detectable t-$ZrO_2$ to m-$ZrO_2$ transformation. The relative fractions of α-$Al_2O_3$, t-$ZrO_2$, and m-$ZrO_2$ remain essentially unchanged. Therefore, the elastic modulus difference between the OCL and the core induced by phase transformation can be neglected in the model. Under the assumptions of linear elasticity, identical elastic modulus for the two regions, and negligible thermal-expansion mismatch (Fig. S6 in the ESM), the residual compressive stress in the surface layer can be written as Eq. (1):

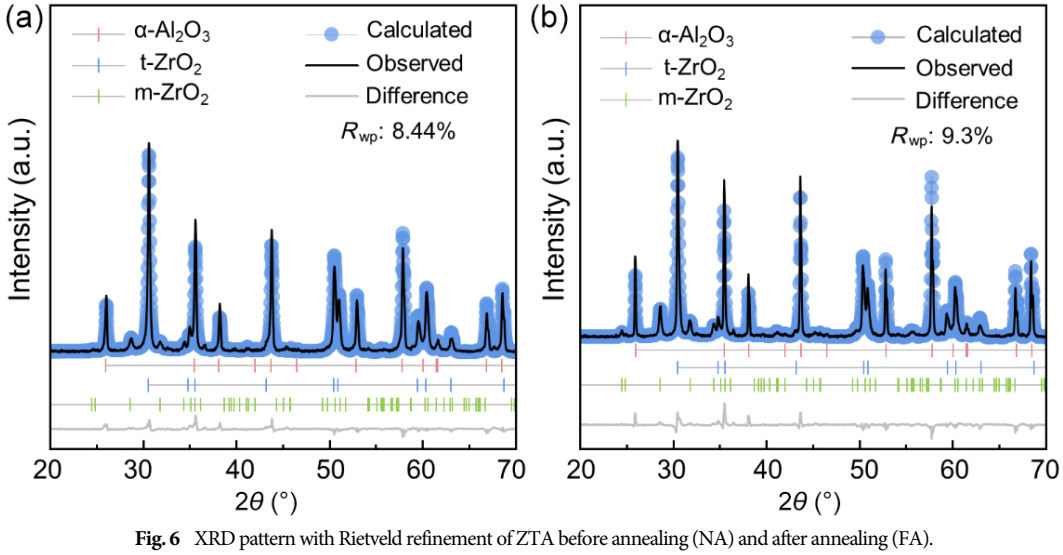



**Fig. 6** XRD pattern with Rietveld refinement of ZTA before annealing (NA) and after annealing (FA).

**Table 1** Refined unit cell parameters of α-$Al_2O_3$ and t-$ZrO_2$ in ZTA

| Phase | Structure | Sample | Lattice parameter, $a$ (Å) | Lattice parameter, $c$ (Å) | Unit-cell volume, $V$ (Å$^3$) |
|---|---|---|---|---|---|
| α-$Al_2O_3$ | Hexagonal | NA | 4.757(9) | 12.991(5) | 254.7(0) |
| | | FA | 4.763(4) | 13.002(9) | 255.5(1) |
| t-$ZrO_2$ | Tetragonal | NA | 3.604(4) | 5.191(3) | 67.44(4) |
| | | FA | 3.607(9) | 5.200(1) | 67.68(9) |

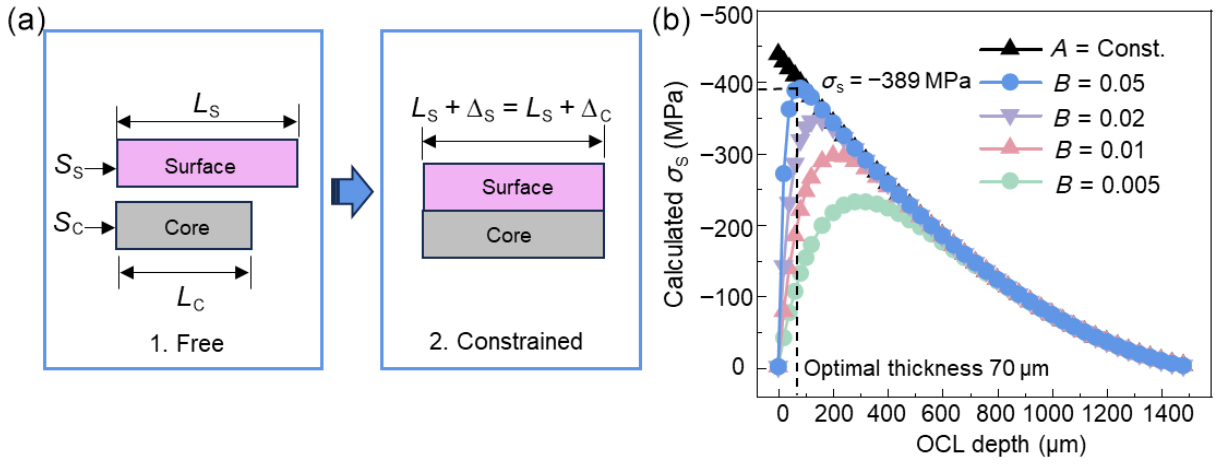



**Fig. 7** (a) Schematic diagram for calculating the dependence of residual surface stress on OCL thickness. (b) Calculated axial pressure stress in OCL.

$$\sigma_s = E\frac{-A}{A+K+1} \quad (1)$$

where $E$ is Young's modulus, and $K = S_s/S_c$ is the cross-sectional area ratio between the surface layer and the core. Here, $A$ represents the linear chemical expansion strain caused by oxygen-vacancy compensation and is the strain term used in Eq. (1). The present specimen geometry can be described by Eq. (2):

$$K = \frac{3\times4}{(3-2d)(4-2d)} - 1 \quad (2)$$

where $d$ denotes the OCL thickness.

Based on XRD-refined lattice expansion, the saturated linear expansion strain was estimated to be $A_0$ = 0.11%. Since oxygen incorporation is progressive rather than instantaneous, especially for thin OCLs, a depth-dependent saturation correction was introduced (Eq. (3)):

$$A = A_0(1 - e^{-Bd}) \quad (3)$$

where $B$ describes the rate of approach to saturation. As shown in Fig. 7(b), the calculated surface compressive stress first increases and then decreases with increasing OCL thickness, in good agreement with the experimentally observed strength evolution. The best experimental strengthening, corresponding to an average flexural-strength increment of 397 MPa at $d = 62.9$ μm, is well matched by the calculated curve with $B = 0.05$. These results support the conclusion that the enhanced flexural strength originates from oxidation-induced expansion of the surface layer and the resulting constraint-generated compressive prestress.

Overall, both the experimental results and the theoretical analysis consistently indicate that oxygen vacancy compensation induces chemical expansion in the surface region, which, under geometric constraints from the inner core, generates a residual compressive stress field responsible for the observed strengthening. Since oxygen vacancy-mediated lattice expansion is a common phenomenon in many oxide ceramics, this surface prestressing strategy based on oxidation-driven defect regulation may be extendable to a broader range of oxide ceramic systems. Compared with conventional coating-based approaches that rely on dissimilar surface layers [11], the present method avoids interfacial compatibility issues and provides a simple, intrinsic route for improving the mechanical performance of oxide ceramics.

## 4 Conclusions

In conclusion, this work demonstrates an OVCP strategy for strengthening ZTA ceramics via defect engineering. Oxygen vacancies introduced during reducing-atmosphere sintering were selectively compensated in the surface region during post-annealing in air, leading to the formation of an oxidized surface layer with residual compressive stress. This treatment increased the flexural strength to (1679±78) MPa, corresponding to a 31% improvement over the unannealed state.

Mechanistically, the strengthening originates from lattice expansion induced by oxygen-vacancy compensation in the surface region. Under constraint from the interior, this expansion is converted into a residual compressive stress field, which suppresses surface-crack initiation during bending. The proposed mechanical model captures the dependence of surface stress on OCL thickness and supports the experimentally observed strengthening trend. More broadly, this defect-regulation-based surface prestressing concept provides a simple and potentially generalizable pathway for enhancing the strength of oxide ceramics.

### Acknowledgements

The authors would like to express their sincere gratitude to Hebei Ruihe Medical Devices Co., Ltd. for its support of this work. This work was supported by the Major Research Plan of the National Natural Science Foundation of China (No. 92263205), the National Natural Science Foundation of China (No. 52502082), and the Beijing Natural Science Foundation Non-Consensus Innovation Project (No. F261029).

### Author contributions

Shile Chen: Writing–original draft, writing–review & editing, methodology, formal analysis. Wenkai Fan: Investigation, writing–original draft, methodology. Liping Chai: Resources, investigation, methodology. Jing Xia: Data curation, funding acquisition. Honghua Li: Conceptualization, writing–review & editing, funding acquisition. Jiangtao Li: Writing–review & editing, supervision, funding acquisition.

### Availability of data and materials

The data that support the findings of this study are available from the corresponding author upon reasonable request.

### Competing interests

The authors have no competing interests to declare that are relevant to the content of this article.

## Electronic Supplementary Material

Supplementary material is available in the online version of this article at https://doi.org/10.26599/JAC.2026.9221346.

## References


[1] Kurtz SM, Kocagöz S, Arnholt C, *et al.* Advances in zirconia toughened alumina biomaterials for total joint replacement. *J Mech Behav Biomed* 2014, **31**: 107–116.

[2] Wang J, Stevens R. Zirconia-toughened alumina (ZTA) ceramics. *J Mater Sci* 1989, **24**: 3421–3440.

[3] Kern F. Relationship between sintering conditions, microstructure and properties of alumina 10 vol% zirconia nanocomposites. *J Ceram Sci Technol* 2012, **3**: 1–7.

[4] Sktani ZDI, Arab A, Mohamed JJ, *et al.* Effects of additives additions and sintering techniques on the microstructure and mechanical properties of zirconia toughened alumina (ZTA): A review. *Int J Refract Met H* 2022, **106**: 105870.

[5] Kuntz M, Krüger R. The effect of microstructure and chromia content on the properties of zirconia toughened alumina. *Ceram Int* 2018, **44**: 2011–2020.

[6] Zhu TB, Xie ZP, Han Y, *et al.* A novel approach to improve flexural strength of $Al_2O_3$–20 wt% $ZrO_2$ composites by oscillatory pressure sintering. *J Am Ceram Soc* 2018, **101**: 1397–1401.

[7] Zhu TB, Xie ZP, Han Y, *et al.* Microstructure and mechanical properties of ZTA composites fabricated by oscillatory pressure sintering. *Ceram Int* 2018, **44**: 505–510.

[8] Yu YD, Zheng YT, Liu XD, *et al.* Making ultra-tough nanoceramics by columnar submicrocrystals with three-level micro-nano structures. *Small* 2022, **18**: 2105367.

[9] Johnston RD, Chipman RD, Knapp WJ. Prestressed ceramics as a structural material. *J Am Ceram Soc* 1953, **36**: 121–126.

[10] Gu JF, Fu S, Ping H, *et al.* Idea of macro-scale and micro-scale prestressed ceramics. *Interdiscip Mater* 2024, **3**: 897–906.

[11] Li HY, Wu HL, Han Y, *et al.* Enhanced high temperature properties of ZTA prestressed ceramics reinforced by cordierite coating. *Int J Appl Ceram Tec* 2024, **21**: 855–860.

[12] Wu HL, Li HY, Cao DK, *et al.* The effects of compressive residual stress on properties of kyanite-coated zirconia toughened alumina ceramics. *Materials* 2023, **16**: 6071.

[13] Bao YW, Kuang FH, Sun Y, *et al.* A simple way to make pre-stressed ceramics with high strength. *J Materiomics* 2019, **5**: 657–662.

[14] Evans AG, Hutchinson JW. The mechanics of coating delamination in thermal gradients. *Surf Coat Tech* 2007, **201**: 7905–7916.

[15] Liu YH, Feng HL, Bao YW, *et al.* Fracture and interfacial delamination origins of bilayer ceramic composites for dental restorations. *J Eur Ceram Soc* 2010, **30**: 1297–1305.

[16] Liu BS, Zhao JL, Chu KL, *et al.* Unraveling the atomic-scale mechanisms of hydrogen defects behavior in yttria-stabilized tetragonal zirconia by first principles calculation. *J Adv Ceram* 2025, **14**: 9221099.

[17] Su XH, Li WJ, Chen D, *et al.* Rapid fabrication of oxygen-deficient zirconia by flash sintering treatment. *J Adv Ceram* 2024, **13**: 1881–1890.

[18] Liu HF, Su HJ, Shen ZL, *et al.* Formation mechanism and roles of oxygen vacancies in melt-grown $Al_2O_3/GdAlO_3/ZrO_2$ eutectic ceramic by laser 3D printing. *J Adv Ceram* 2022, **11**: 1751–1763.

[19] Saggioro ACB, Fernandes L, de Oliveira Carlos Villas-Bôas M *et al.* Processing and characterization of a novel ZTA–MgO for dental applications. *Mater Res* 2025, **28**: 20240404.

[20] Sequeira S, Fernandes MH, Neves N, *et al.* Development and characterization of zirconia–alumina composites for orthopedic implants. *Ceram Int* 2017, **43**: 693–703.

[21] Liu J, Wang Z, Xue Z *et al.* Spontaneous coagulation casting and comprehensive properties of ZTA ceramics. *J Ceram Sci Technol* 2024, **15**: 37–48.

[22] Becher PF, Warwick WH. Fracture strength–fracture resistance response and damage resistance of sintered $Al_2O_3$–$ZrO_2$(12 mol% $CeO_2$) composites. *J Am Ceram Soc* 1994, **77**: 2689–2692.

[23] Norfauzi T, Hadzley AB, Azlan U, *et al.* Fabrication and machining performance of ceramic cutting tool based on the $Al_2O_3$–$ZrO_2$–$Cr_2O_3$ compositions. *J Mater Res Technol* 2019, **8**: 5114–5123.

[24] Zhao W, Wang HB, Chen PC, Rao PG. Preparation of ZTA powders by spray granulation and properties of sintered ZTA composites. *Rare Metal Mat Eng* 2015, **44**: 749–752.

[25] Grigoriev S, Smirnov A, Pinargote NWS, *et al.* Evaluation of mechanical and electrical performance of aging resistance ZTA composites reinforced with graphene oxide consolidated by SPS. *Materials* 2022, **15**: 2419.

[26] Jin XH, Gao L. Effects of powder preparation method on the microstructure and mechanical performance of ZTA/$LaAl_{11}O_{18}$ composites. *J Eur Ceram Soc* 2004, **24**: 653–659.

[27] Kern F. Effect of *in situ*-formed cerium hexaaluminate precipitates on properties of alumina–24 vol% zirconia (1.4Y) composites. *J Ceram Sci Technol* 2013, **4**: 177–185.

[28] Zhou J, Jiang SH, Yang JP *et al.* Effect of SrO precursors on the microstructure and mechanical properties of zirconia-toughened alumina (ZTA) composites. *J Ceram Sci Technol* 2026, **17**: 53–62.

[29] Goto K, Hirota K, Yamaguchi O, *et al.* Formation and sintering of 75 mol% alumina/25 mol% zirconia (2–3.5 mol% yttria) composite powder prepared by the hydrazine method. *J Mater Sci* 1996, **31**: 204–208.

[30] Fan WJ, Li HB, Zhao FY, *et al.* Boosting the photocatalytic performance of (001) BiOI: Enhancing donor density and separation efficiency of photogenerated electrons and holes. *Chem Commun* 2016, **52**: 5316–5319.